Morphology and Lateral Strain Control of Pt Nanoparticles *via* Core–Shell Construction Using Alloy AgPd Core Toward Oxygen Reduction Reaction

Jinhua Yang, Jun Yang,[‡] and Jackie Y. Ying*

Institute of Bioengineering and Nanotechnology, 31 Biopolis Way, The Nanos, Singapore 138669. [‡]Present address: Institute of Process Engineering, Chinese Academy of Sciences, Beijing, China 100190.

ABSTRACT Controlling the morphology of Pt-based nanomaterials can be an effective way to improve the catalytic activity on a mass basis. Herein we demonstrate for the first time the synthesis of monodispersed core–shell AgPd@Pt nanoparticles with multiply twinned structures. These multiply twinned particles (MTPs), which possess the icosahedra structure, exhibit superior catalytic activity toward oxygen reduction reaction (ORR) in fuel cells. The Ag component of the alloy AgPd inner core is crucial for the construction of the multiply twinned structure of the core–shell nanoparticles, while the Pd component is used to reduce the tensile strain effect of the Ag on the deposited Pt layers, rendering the Pt binding energy in core–shell AgPd@Pt MTPs to be close to that of commercial Pt nanoparticles. The enhanced ORR activity of AgPd@Pt/C can be explained in terms of a much higher surface fraction of atoms on the (111) facets for icosahedral MTPs. This core–shell structure offers an interesting example to investigate the morphology and lateral strain effect of the substrate on the deposited layers, and their influence on the catalytic activity of metal catalysts.

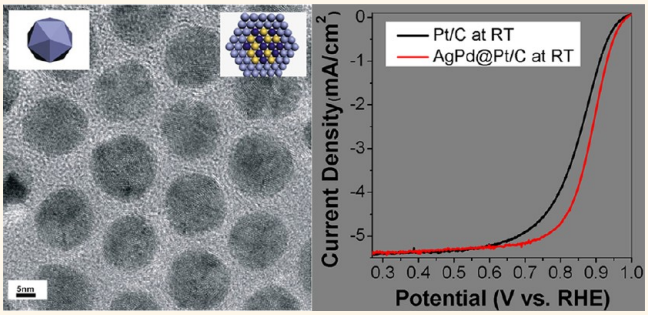

KEYWORDS: platinum · core–shell · multiply twinned particles · lateral strain · oxygen reduction reaction

The synthesis of nanostructured materials with superior catalytic performance is of great interest.[1−4] The size- and shape-dependent properties of nanoparticles are well-known and have been exploited in various applications.[3,5] Nanoparticles could be prepared as single crystals or particles with controlled multiply twinned structures and well-defined crystallographic faces, allowing for the tuning of catalytic activities.[6−8] Platinum (Pt) nanoparticles with controlled morphologies, such as tetrahedral,[1] cubic,[9−11] truncated octahedral[2] and high-index tetra-hexahedrons,[6] have been demonstrated as highly active catalysts for various reactions. Icosahedral nanoparticles with a high density of compressed twins on the surfaces are expected to be the most active catalysts.[12] The excellent activity of the multiply twinned particles (MTPs) of Pt with (111) facet of icosahedral morphology with a high density of twins and corners on their surface was also verified computationally.[13] However, unlike palladium (Pd),[12] silver (Ag),[4] and gold (Au),[14] MTPs of Pt were rarely formed.[15]

Fuel cells, such as polymer electrolyte membrane fuel cells (PEMFCs), are promising as a power source in stationary and portable applications. However, the high costs associated with the Pt catalyst loading in the cathode have hampered the commercialization of PEMFCs.[16,17] The challenge lies with the slow kinetics of the oxygen reduction reaction (ORR), which requires a significant amount of Pt catalysts for high catalytic performance.[18−20] A number of approaches/techniques have been developed to resolve these critical issues for improving the performance of Pt-based electrocatalysts for ORR in PEMFCs. The most common practice is to prepare Pt-based electrocatalysts with a hollow interior or porous nanostructure,[21−31] which have been demonstrated to have higher ORR activities than pure Pt particles. Recently,

* Address correspondence to jyying@ibn.a-star.edu.sg.

Received for review June 21, 2011 and accepted October 12, 2012.

Published online October 12, 2012
10.1021/nn303298s

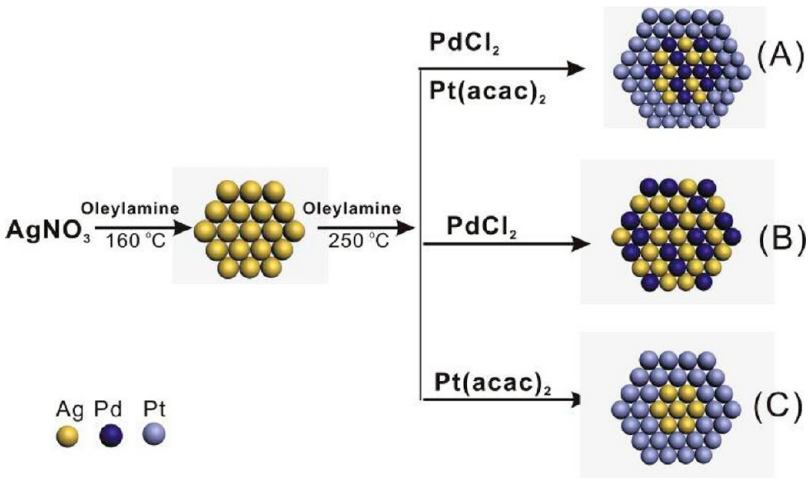

Scheme 1. Seed-mediated growth synthesis of nanocrystalline MTPs of (A) AgPd@Pt, (B) AgPd, and (C) Ag@Pt, with icosahedral morphology.

enhanced ORR catalytic activity has also been achieved by Pt-on-Pd heteronanostructures or nanodendrites.[17,20] The synthesis of such electrocatalysts starts with the preparation of Pd cores through wet chemistry. Pt nanoparticles are grown subsequently onto the Pd cores. Although these nanostructures have displayed excellent catalytic properties, the lack of strategies to maintain their complex structures after long-term use has limited their commercial applications.

To enhance the catalytic activities while reducing Pt loading, core–shell materials with different shapes/morphologies may be applied toward ORR. They could be prepared by ultrahigh vacuum (UHV) approaches[32] or *via* chemical syntheses (*e.g.*, surface metal galvanic displacement,[12,33,34] surface metal depletion gliding,[35,36] and seed-mediated growth[37–40]). For example, Sun and co-workers prepared core–shell Pd@FePt nanoparticles with a 5-nm Pd core and a FePt shell of tunable thickness (1–3 nm), and found that the FePt shell of 1 nm-thick exhibited significantly higher durability and ORR activity.[39] Herein, we reported for the first time the synthesis of monodispersed core–shell AgPd@Pt MTPs with icosahedral morphology (Scheme 1A), and investigated their application in catalyzing ORR at room and moderate temperatures. In this method, oleylamine was used as solvent, reducing agent, and stabilizer for the formation of nanoparticles. The Ag component of the AgPd alloy inner core was crucial for the construction of the multiply twinned structure of the core–shell nanoparticles, while the Pd component was employed to reduce the tensile strain effect of the Ag on the deposited Pt layers. The core–shell AgPd@Pt MTPs exhibited superior catalytic activity toward ORR, as compared to the commercial Pt nanoparticles. The enhancement was attributed to the higher surface fraction of atoms on the (111) facets of icosahedral Pt MTPs.

RESULTS AND DISCUSSION

In the first step, a simple one-pot method was employed to synthesize Ag nanoparticles. A transmission electron microscopy (TEM) image of Ag nanoparticles synthesized at 160 °C in the oleylamine solution containing 26 mM $AgNO_3$ is shown in Figure 1A. The nanoparticles have an average diameter of ~7.0 nm. The high-resolution TEM (HRTEM) image illustrated that the Ag nanoparticles were multiply twinned with an icosahedral morphology.[14,41,42] These Ag MTPs were then used as seeds for the formation of core–shell nanoparticles.

To prepare AgPd@Pt MTPs, $PdCl_2$ and $Pt(acac)_2$ were immediately added to Ag colloidal solution, which was kept at 250 °C for 1 h under a nitrogen flow with magnetic stirring. Upon the addition of Pd(II) and Pt(II) salts, the replacement reaction between Ag nanoparticles and Pd(II) occurred immediately to form AgPd alloy nanoparticles, analogous to the formation of AgAu or AgPd alloy nanoparticles by replacement reaction between Ag nanoparticles and Au or Pd metal ions in aqueous solution.[43] The alloying process was realized by the rapid interdiffusion of metal atoms as a result of the reduced dimension of the silver templates, the elevated temperature, and the large number of interfacial vacancy defects generated by the replacement reaction. Besides the replacement reaction between Ag and Pd, the extra Ag (I) and Pd (II) species would be reduced by oleylamine at a high temperature (250 °C). The subsequent reduction of Pt(II) precursors resulted in the homogeneous deposition of Pt on the preformed AgPd alloy nanoparticles. The as-prepared colloidal solution was then cooled to room temperature, and the nanoparticles were precipitated, washed with methanol, and redispersed in nonpolar organic solvents (*e.g.*, toluene, hexane, and chloroform). The Ag:Pd:Pt molar ratio in the final product AgPd@Pt/C was very close to the precursor molar ratio used, as

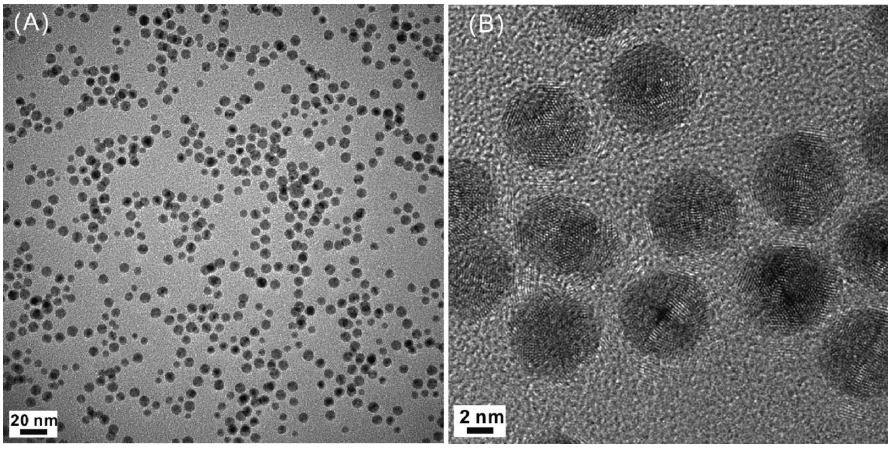

Figure 1. (A) TEM and (B) HRTEM images of icosahedral Ag nanoparticles. The average particle diameter was 7.0 ± 0.8 nm.

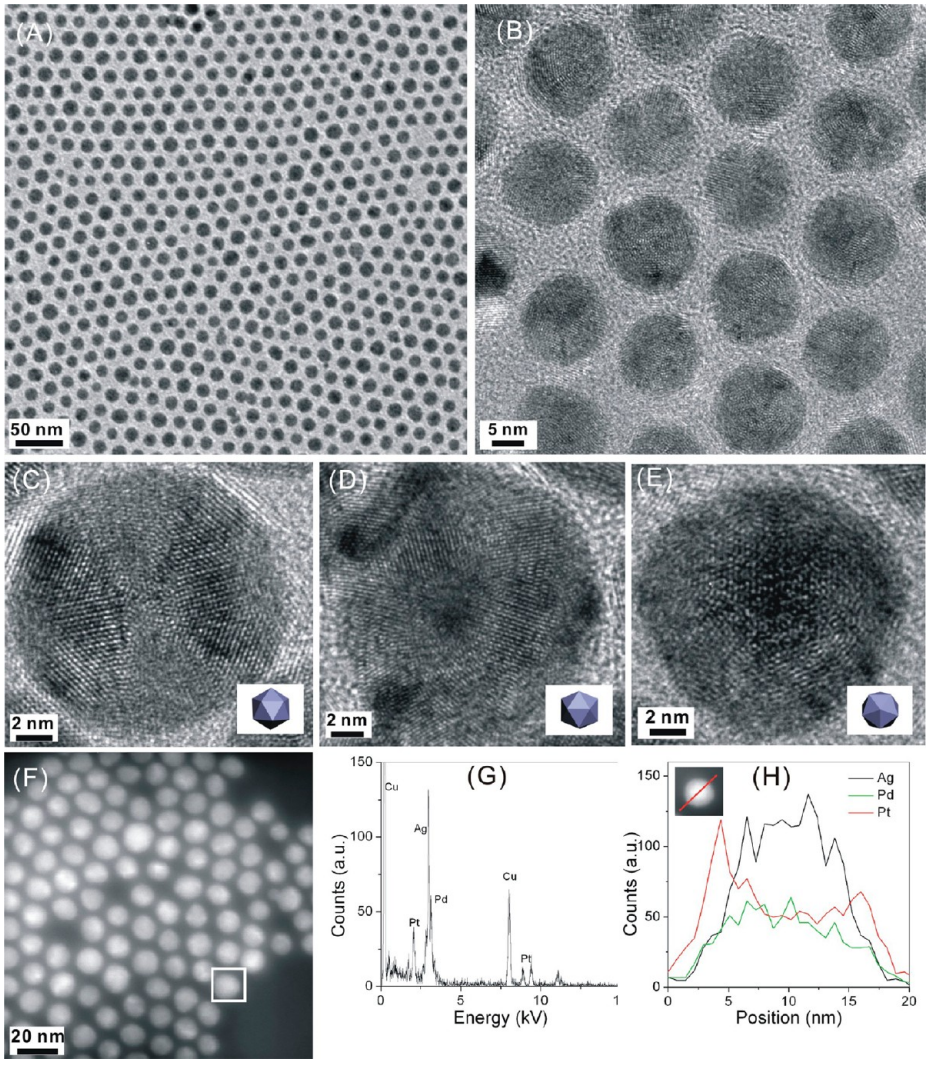

Figure 2. (A) TEM and (B) HRTEM images of icosahedral core−shell AgPd@Pt nanoparticles. HRTEM images of AgPd@Pt MTP along a (C) 2-fold, (D) 3-fold, and (E) 5-fold symmetry axis; (F) HAADF-STEM image; (G) EDX spectrum of a single AgPd@Pt MTP boxed in (F); (H) Ag, Pd and Pt elemental profiles along the red line across the MTP (inset of H).

confirmed by ICP−MS results (see Supporting Information (SI) Table S1). A typical TEM image of the core−shell AgPd@Pt nanoparticles is shown in Figure 2A. The nanoparticles were nearly monodispersed, with an average size of ~15 nm. The narrow size distribution of nanoparticles resulted in the formation of

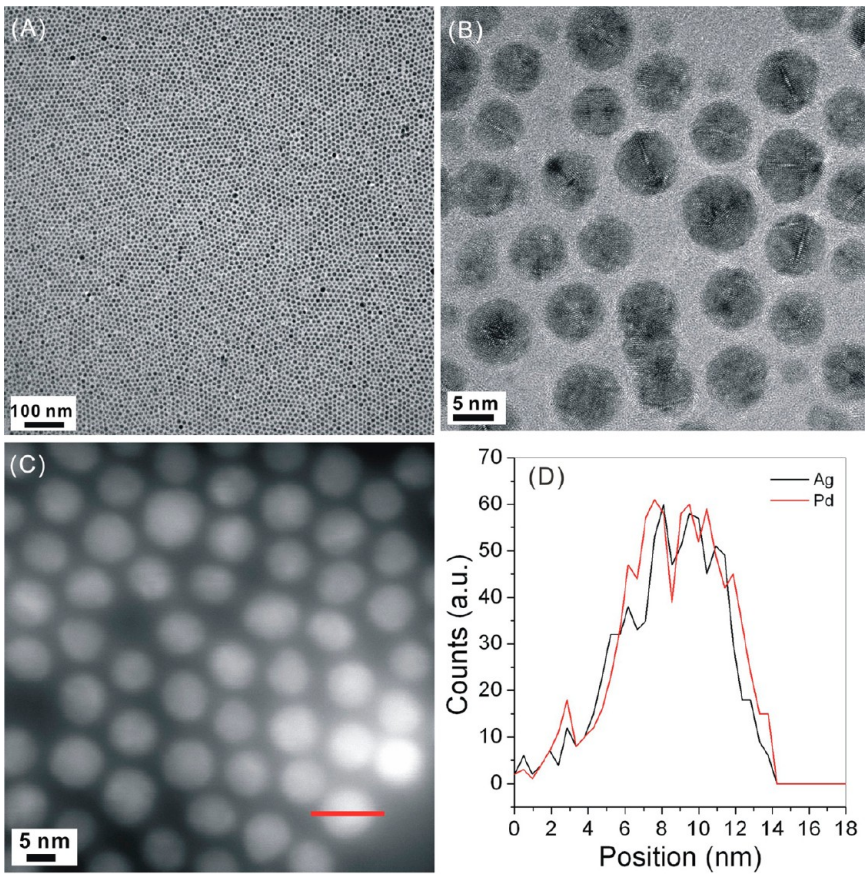

Figure 3. (A) TEM, (B) HRTEM, and (C) HAADF-STEM images of AgPd nanoparticles; (D) Ag and Pd elemental profiles along the red line across the AgPd nanoparticle shown in panel C.

two-dimensional close-packed hexagonal arrays on the TEM grid. The core–shell AgPd@Pt nanoparticles were predominantly multiply twinned with an icosahedral morphology, as illustrated by the HRTEM image (Figure 2B and SI Figure S1). They were found in different orientations (along a 2-fold symmetry axis in Figure 2C, along a 3-fold symmetry axis in Figure 2D, and along a 5-fold symmetry axis in Figure 2E).[14,41,42] The energy dispersive X-ray (EDX) spectroscopy analysis (Figure 2G) of an arbitrary single particle boxed in the high-angle annular dark-field scanning transmission electron microscopy (HAADF-STEM) image of Figure 2F confirmed that the particle was indeed composed of Ag, Pd, and Pt. Since the lattice mismatch between the AgPd alloy core and the Pt shell was only ~1.1% (as calculated from the X-ray diffraction (XRD) patterns in SI Figure S2),[44] the core–shell nanoparticles were difficult to determine accurately using standard TEM. However, the formation of core–shell AgPd@Pt nanoparticles could be confirmed by the elemental profiles of these particles. As shown in Figure 2H and SI Figure S3, the Pt signal was noted across the entire particle (~15 nm), whereas the Ag and Pd signals were obtained only across the core (~10 nm).

Pt 4f X-ray photoelectron spectroscopy (XPS) was conducted on the core–shell AgPd@Pt/C nanoparticles (SI Figure S4), and the results of peak deconvolution are summarized in SI Table S2. Figure S4a shows the Pt 4f region of the Pt/C spectrum, which could be deconvoluted into two pairs of doublets. The most intense doublet (at 71.00 and 74.38 eV) was characteristic of metallic Pt. The second and weaker doublet (at 72.30 and 75.63 eV) could be assigned to Pt in oxidized forms, such as PtO and $Pt(OH)_2$. Similarly, the Pt 4f region of the AgPd@Pt spectrum (Figure S4C) could be deconvoluted into a doublet at 71.12 and 74.43 eV assignable to Pt (0), and a doublet at 72.36 and 75.75 eV due to Pt oxide. The zeroval-ent metallic state of Pt featured prominently in AgPd@Pt/C (76.5%) and in Pt/C (77.8%). A slight shift in the Pt binding energy was observed in AgPd@Pt as compared with Pt/C, which might be attributed to the larger particle size of core–shell AgPd@Pt nanoparticles. It was also noted that Pt (2.28) has a slightly higher electronegativity than Ag (1.93) and Pd (2.20), and hence Pt could, in principle, withdraw electrons from the neighboring Pd atoms in core–shell AgPd@Pt/C. This effect would result in a shifting of the binding energies. In addition, the shift in Pt binding energy might also be caused by the slight strain effect imposed by the alloy AgPd core on the Pt shell.[45]

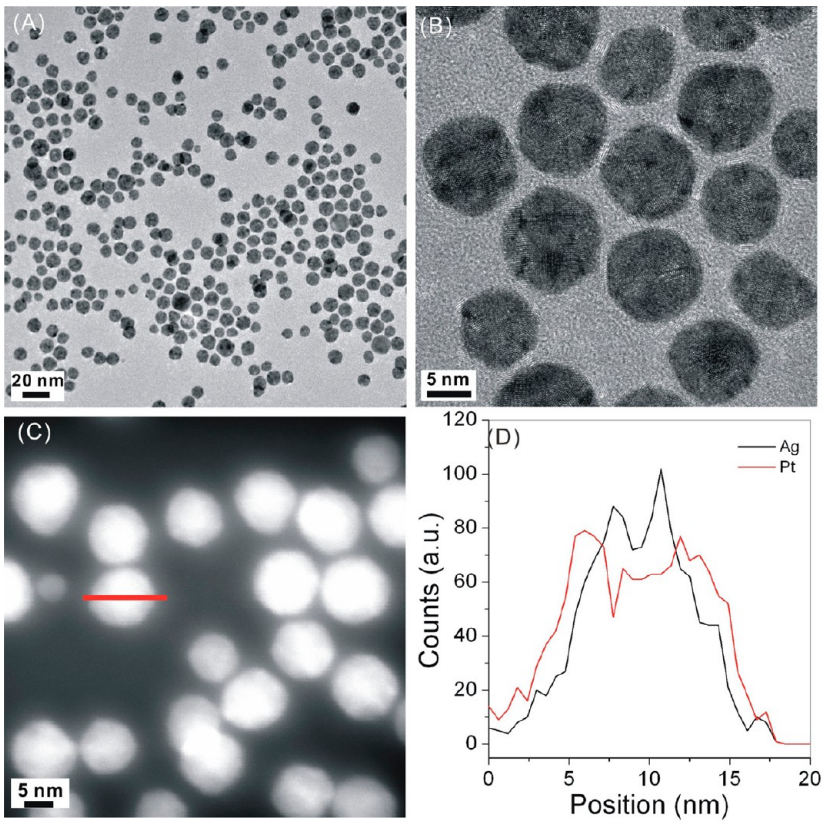

Figure 4. (A) TEM, (B) HRTEM, and (C) HAADF-STEM images of Ag@Pt nanoparticles; (D) Ag and Pt elemental profiles along the red line across the Ag@Pt nanoparticle shown in panel C.

The addition of Pd(II) alone or Pt(II) alone to icosahedral Ag seeds was also investigated (Scheme 1B,C). This resulted in AgPd alloy nanoparticles of ~10 nm (Figure 3) or core–shell Ag@Pt nanoparticles of ~12 nm (Figure 4), respectively. The AgPd alloy and core–shell Ag@Pt nanoparticles were predominantly multiply twinned with an icosahedral morphology, as illustrated by the HRTEM image (Figures 3B and 4B). The AgPd alloy (Figure 3C,D) and core–shell Ag@Pt (Figure 4C,D) structures were confirmed by EDX analysis of an arbitrary single particle boxed in the respective HAADF-STEM images. The XRD patterns of Ag, AgPd alloy, core–shell Ag@Pt, core–shell AgPd@Pt, and Pt nanoparticles prepared in oleylamine were presented in SI Figure S2. As compared to pure Pt nanoparticles, a shift to a lower angle was observed for the (111) diffraction peak of core–shell Ag@Pt (SI, Figure S2C). This is because Ag has larger lattice parameter (0.4090 nm) than that of Pt (0.3923 nm), and the Ag cores exert a tensile effect on the Pt atoms deposited on their surface. In contrast, the (111) diffraction peak of AgPd@Pt was very close to that of pure Pt, indicating that the presence of Pd in AgPd cores could reduce the tensile effect induced by Ag on the Pt layer. Based on the calculation from Figure S2B, the lattice parameter for the (111) facet of AgPd alloy was 0.3967 nm, very similar to that of pure Pt.

For the electrochemical characterizations, the core–shell AgPd@Pt nanoparticles were loaded on Vulcan XC-72 carbon supports. TEM and HRTEM images of the AgPd@Pt/C nanoparticles showed that the core–shell AgPd@Pt nanoparticles were well dispersed on XC-72, maintaining their particle size, narrow size distribution, and multiply twinned structure with icosahedral morphology (Figure 5).

The catalytic activity of the core–shell AgPd@Pt MTPs with icosahedral morphology toward ORR was evaluated by sweep voltammetry in O_2-saturated $HClO_4$, and benchmarked against that of the commercial spherical Pt nanoparticles (average diameter, ~3 nm) (SI Figure S5). Cyclic voltammograms of Pt/C and AgPd@Pt/C in argon-purged 0.1 M $HClO_4$ at room temperature were used to obtain electrochemically active surface areas (ECSAs) from the hydrogen adsorption/desorption regions (0.00–0.30 V *vs* reversible hydrogen electrode (RHE) in Figure 6A). In the cathodic scan, the oxide (OH_{ads}) stripping peak (0.80 V) for AgPd@Pt/C was higher than that for Pt/C (0.78 V). The positive shift of ~0.02 V in the oxide stripping peak for AgPd@Pt/C suggested a weaker binding of the OH_{ads} species on this catalyst's surface.[16] This could be attributed to a weaker interaction with the adsorbed species on the dominant (111) facets.[46] Figure 6B shows the ORR polarization curves of these two catalysts in oxygen-saturated 0.1 M $HClO_4$ at room temperature and 60 °C. The results are summarized in SI Table S3. For the pure Pt nanoparticles, the ECSA would

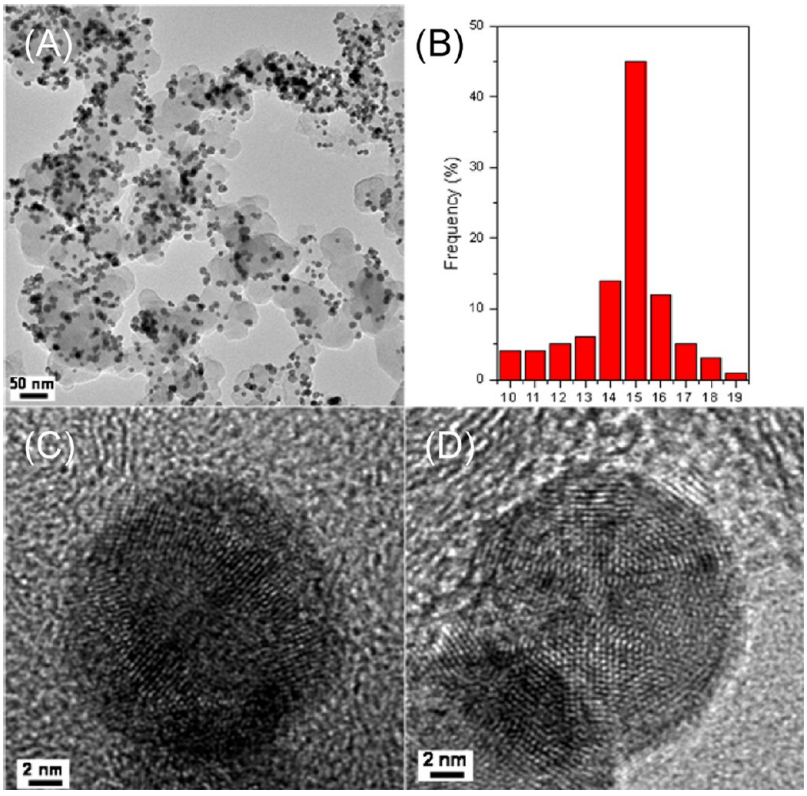

Figure 5. (A) TEM image and (B) size distribution (in nm) of AgPd@Pt/C catalysts; HRTEM images of a single AgPd@Pt icosahedral nanoparticle supported on XC-72 carbon along a (C) 2-fold and (D) 5-fold symmetry axis.

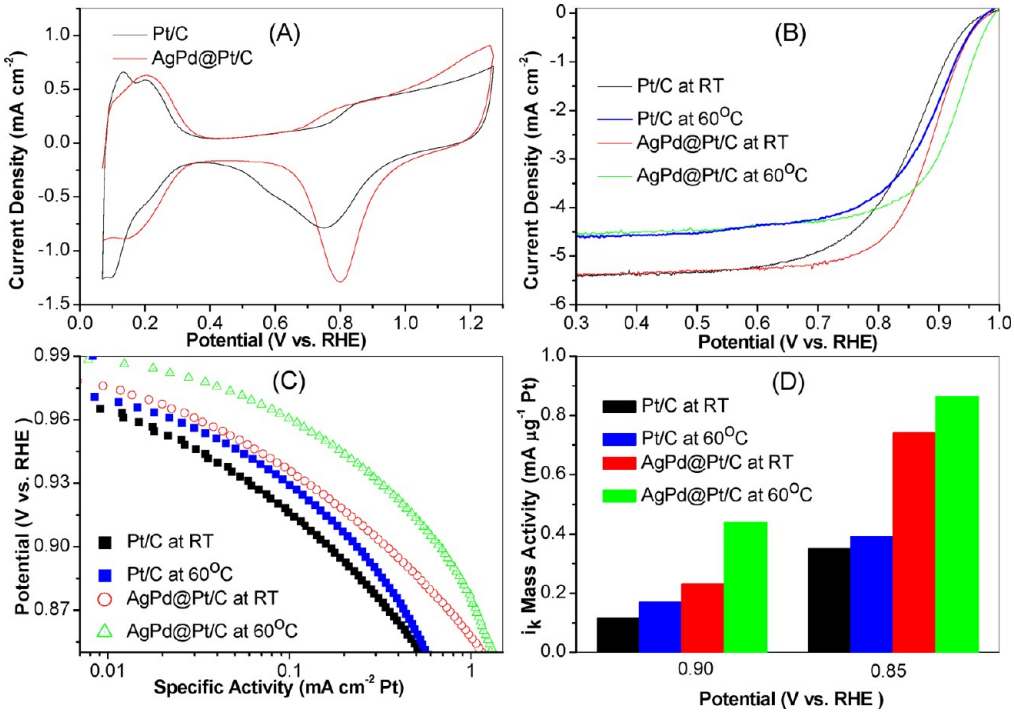

Figure 6. (A) Cyclic voltammograms of Pt/C and AgPd@Pt/C in argon-purged 0.1 M $HClO_4$; sweep rate = 20 mV/s, room temperature. (B) Linear sweep voltammograms in oxygen-saturated 0.1 M $HClO_4$ showing the positive-going scans; sweep rate = 20 mV/s, room temperature or 60 °C, 1600 rpm. (C) Tafel plot for ORR at high potential, normalized by Pt ECSA. (D) Kinetic mass activities of ORR at 0.85 and 0.90 V RHE, normalized by Pt mass.

decrease with increasing particle size.[16] In this work, the slightly smaller ECSA of 15-nm AgPd@Pt/C than the commercial 3-nm Pt/C was attributed to the core–shell structure of AgPd@Pt nanoparticles with multiply

twinned icosahedral morphology. At room temperature, AgPd@Pt/C showed a more positive half-wave potential (0.88 V) than Pt/C (0.86 V), indicating that it has a higher ORR activity.

By normalizing the Pt surface area, the specific activities of AgPd@Pt/C and Pt/C were obtained (Figure 6C). At room temperature and 0.9 V *vs* RHE, a specific activity of 0.357 mA/cm^2 Pt was attained for AgPd@Pt, which was >2 times higher than that for Pt/C (0.160 mA/cm^2 Pt). Kinetic mass activity calculated from the Koutecký–Levìch equation (Figure 6D) also confirmed that AgPd@Pt (0.230 mA/μg Pt) was superior to Pt/C (0.113 mA/μg Pt). Furthermore, regardless of whether Pt surface area or Pt mass was used as the basis for normalizing the measured current, the specific activity (0.680 mA/cm^2 Pt) and mass activity (0.439 mA/μg Pt) of AgPd@Pt/C at 60 °C and 0.90 V were higher than that of commercial Pt (0.239 mA/cm^2 Pt and 0.168 mA/μg Pt, respectively). The former values were also close to the 2015 targets set by the U.S. Department of Energy (DoE) at 80 °C and 0.9 V (0.72 mA/cm^2 Pt and 0.44 mA/μg Pt, respectively). Even on the basis of total mass of Pd and Pt, our AgPd@Pt catalyst showed greater mass activities at room temperature and 60 °C (0.148 mA/μg Pt+Pd and 0.282 mA/μg Pt+Pd, respectively) than the commercial Pt catalyst (0.113 mA/μg Pt, and 0.168 mA/μg Pt, respectively).

The catalytic activities of AgPd alloy and core–shell Ag@Pt nanoparticles toward ORR were found to be much lower than that of the core–shell AgPd@Pt nanoparticles (SI Figure S6). It is well-known that most Pd-based catalysts are lower in intrinsic ORR activities than Pt.[47,48] Therefore, it was not unexpected that the AgPd alloy nanoparticles showed a lower activity than Ag@Pt and AgPd@Pt nanoparticles. For the Ag@Pt nanoparticles, the tensile effect of Ag core on the Pt shell would result in an upward shift of the d-band center of Pt.[49] It is generally accepted that the common ORR process, that is, the series 4-electron pathway, must involve both the breaking of an O–O bond and the formation of O–H bonds.[18,32,50] The most active Pt-based catalyst should have the d-band center with an intermediate value since the optimal ORR catalyst needs to facilitate both bond-breaking and bond-making steps without hindering one or the other.[51,52] As has been demonstrated,[53] the surface of a Pt-based catalyst with a high value in d-band center tends to bind adsorbents more strongly, enhancing the kinetics of dissociation reactions producing these adsorbents. Compared to the core–shell Ag@Pt nanoparticles, the core–shell AgPd@Pt nanoparticles showed superior catalytic activity toward ORR possibly because they have a more suitable d-band center to balance the breaking of O–O bonds and the formation of O–H bonds.

Classical Koutecký–Levìch plots for Pt/C and AgPd@Pt/C catalysts are shown in SI Figure S7. These plots are presented as i^{-1} *vs* $f^{-1/2}$, where the relationship between ω (angular frequency of rotation) and f (frequency in rpm) is given by $\omega = 2\pi f/60$. The number of electrons transferred in the first-order reduction reaction, n, can be obtained from the Koutecký–Levìch equation.[54] The Koutecký–Levìch plots all yielded straight lines, from which n values for Pt/C and AgPd@Pt/C were calculated to be 3.87 and 3.77, respectively (SI Figure S7). This indicated that ORR over AgPd@Pt/C catalysts occurred by the same 4-electron reaction pathway as that over Pt.

The enhancement of ORR activity through a shape-controlled strategy might be understood in terms of a high surface fraction of atoms on the (111) facets for the multiply twinned icosahedral structure. Surface studies have shown that ORR activity increased in the order of (100) < (110) ~ (111) in perchloric acid for the three low-index facets of Pt.[46,55] It was calculated that the (111) facets would represent >80% and ~30% of the total surface for 15-nm AgPd@Pt MTPs with icosahedral structure and 3-nm spherical Pt nanoparticles,[12] respectively. The dominance of the (111) facets in AgPd@Pt MTPs would account for its high ORR activity. It is well-known that there are various pathways for ORR, but all ORR involves both the dissociation of the O–O bond and the removal of the surface OH groups as the basic elementary steps, regardless of the detailed mechanisms. The strong adsorption of intermediate OH_{ads} on the catalyst surface has a negative impact on the performance of Pt-based catalysts.[18,46,54] Therefore, the enhanced catalytic activity for ORR over icosahedral nanoparticles could be attributed to the structure-sensitive adsorption of the intermediate OH_{ads} species in the reaction. The (111) facets of the icosahedral structure has the lowest coverage by OH_{ads}, and the weakest Pt–OH_{ads} interaction, giving rise to the highest activities among the three low-index facets ((111), (110) and (100)).

Furthermore, chronoamperometry of Pt/C and AgPd@Pt/C at 0.87 V in oxygen-saturated 0.1 M $HClO_4$ was used to obtain "steady-state" activities after 2 h. Figure 7 shows that the ORR current density of Pt/C decreased to ~0.07 mA/cm^2 after 2 h. In contrast, the "steady-state" specific activity of AgPd@Pt/C was much higher (0.17 mA/cm^2). Figure 7 also shows that the rate of decrease in ORR current density was smaller for AgPd@Pt/C than for Pt/C, indicating the greater stability of the MTPs. The (111)-rich icosahedral AgPd@Pt MTPs were more resistant against deactivation as they have fewer low-coordination sites that were prone to oxidation and dissolution.[12,56] After the chronoamperogram experiment, the nanoparticles maintained their multiply twinned structure (SI Figure S8).

Thus, this study provided experimental evidence for enhancing the ORR activity of Pt through morphological control. The design of AgPd@Pt MTPs with icosahedral structure could be further optimized in future

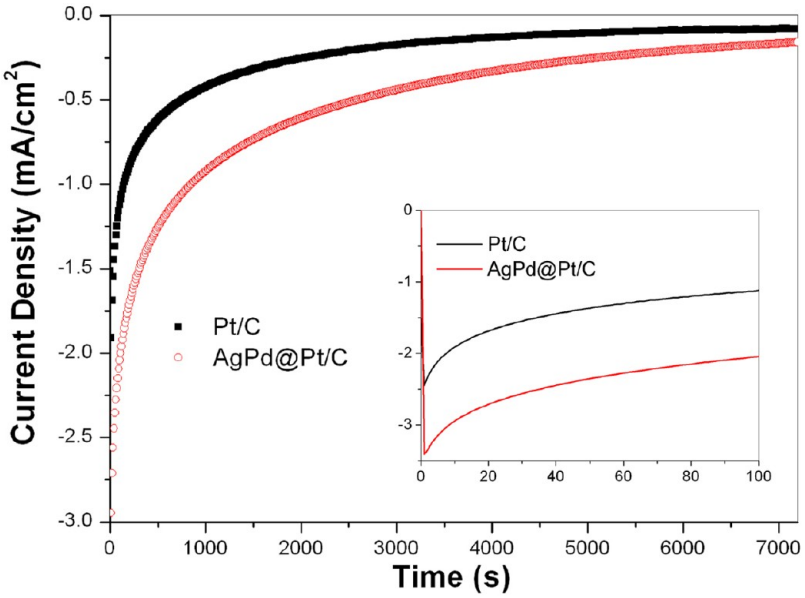

Figure 7. Chronoamperograms of Pt/C and AgPd@Pt/C at 0.87 V RHE in oxygen-saturated 0.1 M $HClO_4$; room temperature, 1600 rpm. The inset shows the enlarged graph for the first 100 s.

investigations. For example, decreasing the particle size could further improve the ORR activity, and reducing the thickness of Pt shell would provide further cost savings.

CONCLUSION

Monodispersed AgPd@Pt MTPs with icosahedal structure can be obtained by reducing platinum precursors in oleylamine in the presence of preformed AgPd alloy nanoparticles. The Ag component of the AgPd inner core is critical toward the construction of the multiply twinned structure of the core–shell nanoparticles. The Pd component acts to effectively reduce the tensile strain effect of Ag on the deposited Pt layers, rendering the Pt binding energy in the core–shell AgPd@Pt MTPs to be close to that of commercial Pt nanoparticles. The multiply twinned AgPd@Pt nanoparticles exhibit superior catalytic activity toward ORR in fuel cells due to the high surface fraction of Pt atoms on the (111) facets of icosahedral MTPs. This complex nanostructure design demonstrates the possibility to manipulate the morphology and lateral strain effects of the substrate on the deposited layers, and their impact on significantly improving the catalytic activity of metal catalysts.

METHODS

Chemicals. Silver nitrate ($AgNO_3$, 99.9%), palladium chloride ($PdCl_2$, 99.9%), platinum(II) acetylacetonate ($Pt(acac)_2$, 97%), oleylamine (technical grade, 70%), methanol (98%), and toluene (99%) from Sigma-Aldrich, aqueous $HClO_4$ solution (70%, ACS reagent), commercial Pt/C catalysts (20 wt % of Pt nanoparticles (3.2 nm) on Vulcan XC-72 carbon support) from E-TEK, and Vulcan XC-72 carbon powders (BET surface area = 250 m^2/g and average particle size = 40–50 nm) from Cabot were used as received. All glassware and Teflon-coated magnetic stir bars were cleaned with aqua regia, followed by copious rinsing with deionized water before drying in an oven.

Synthesis of Ag, AgPd Alloy, Core–Shell Ag@Pt, and Core–Shell AgPd@Pt MTPs. In a typical synthesis of Ag MTPs, a solution of 45 mg of $AgNO_3$ in 10 mL of oleylamine was heated at 160 °C in a nitrogen atmosphere under magnetic stirring for 1 h. These Ag nanoparticles were then used as seeds for the formation of alloy or core–shell nanoparticles. For the synthesis of AgPd alloy MTPs, 30 mg of $PdCl_2$ was immediately added to the above Ag MTPs solution, and the mixture was heated at 250 °C for 1 h under a nitrogen flow with rapid magnetic stirring. For core–shell Ag@Pt MTPs synthesis, 65 mg $Pt(acac)_2$ was immediately added to the Ag seed solution, and the mixture was kept at 250 °C for 1 h under a nitrogen flow with magnetic stirring. For core–shell AgPd@Pt MTPs synthesis, 30 mg of $PdCl_2$ and 65 mg of $Pt(acac)_2$ were added immediately to the Ag seed solution, and the mixture was kept at 250 °C for 1 h in a nitrogen atmosphere under magnetic stirring. The resulting MTPs were then cooled to room temperature. The nanoparticles in the solution were precipitated by methanol, and washed twice with methanol to remove the free ligands, followed by redispersion in toluene. For catalyst loading on Vulcan XC-72 carbon support, 40 mg of carbon was added to the solution of MTPs (AgPd, Ag@Pt, and AgPd@Pt). After 24 h of stirring, MTP/C catalysts (with 20 wt % Pd loading for AgPd, and 20 wt % Pt loading for Ag@Pt and for AgPd@Pt) were collected *via* centrifugation, and washed three times with methanol. They were then dried at room temperature in vacuum.

Materials Characterization. The products were characterized by TEM, HRTEM, and HAADF-STEM (FEI Tecnai G^2 F20 electron microscope). Samples for TEM examination were prepared by putting a droplet of the treated solution on a copper grid coated with a thin carbon film, and then evaporating the droplet in air at room temperature. The catalyst composition was determined *in situ* by an EDX attachment to the microscope. XRD patterns were recorded on a Rigaku D/Max-3B diffractometer using Cu Kα radiation (λ = 1.54056 Å). XPS spectra were obtained with an ESCALAB MKII spectrometer (VG Scientific) using Al–Kα radiation (1486.71 eV). Samples for XRD and XPS measurements were precipitated from a toluene solution of the nanoparticles using methanol, recovered *via* centrifugation, and washed with

methanol several times to remove nonspecifically bonded oleylamine. The nanoparticles were then dried at room temperature in vacuum.

Electrochemical Measurements. Electrochemical measurements were conducted in a standard three-electrode cell. Pt gauze and Ag/AgCl (3 M KCl) were used as the counter electrode and the reference electrode, respectively. A thin layer of Nafion-impregnated catalyst cast on a vitreous carbon disk was used as the working electrode. A calculated volume of the catalyst ink (10 mg of ultrasonically dispersed catalyst in 10 mL of aqueous solution containing 4 mL of isopropyl alcohol and 0.2 mL of 5 wt % Nafion solution) was dispensed onto a 5-mm glassy carbon disk electrode to give a nominal catalyst loading of 15 μg of Pt per cm^2 of the electrode projection area. All potentials were converted to the RHE scale, and current densities were normalized by the projection area of the 5 mm-diameter electrode. ORR activities were measured in 0.1 M $HClO_4$ electrolyte. Positive-going linear sweep voltammograms were recorded from 1.0 to 0 V at 20 mV/s at room temperature (25 $\pm$ 2 °C) and 60 °C. Cyclic voltammograms were also recorded between 0 and 1.2 V at 20 mV/s and room temperature in 0.1 M $HClO_4$ for the measurement of the ECSAs.

Conflict of Interest: The authors declare no competing financial interest.

Acknowledgment. This work was funded by the Institute of Bioengineering and Nanotechnology (Biomedical Research Council, Agency for Science, Technology and Research, Singapore).

Supporting Information Available: TEM images of commercial Pt/C catalysts, HRTEM and HAADF-STEM images of AgPd@Pt, TEM and HRTEM images of AgPd@Pt/C after chronoamperometry testing, XRD, XPS, linear sweep voltammograms and Koutecký–Levich plots of the catalysts, molar ratios in catalysts obtained from ICP–MS and point-resolved EDX measurements, and Pt loading in catalyst based on the ICP–MS results. This material is available free of charge *via* the Internet at http://pubs.acs.org.

REFERENCES AND NOTES

1. Narayanan, R.; El-Sayed, M. A. Shape-Dependent Catalytic Activity of Platinum Nanoparticles in Colloidal Solution. *Nano Lett.* **2004**, *4*, 1343–1348.
2. Narayanan, R.; El-Sayed, M. A. Changing Catalytic Activity during Colloidal Platinum Nanocatalysis Due to Shape Changes: Electron-Transfer Reaction. *J. Am. Chem. Soc.* **2004**, *126*, 7194–7195.
3. Narayanan, R.; Tabor, C.; El-Sayed, M. A. Can the Observed Changes in the Size or Shape of a Colloidal Nanocatalyst Reveal the Nanocatalysis Mechanism Type: Homogeneous or Heterogeneous? *Top. Catal.* **2008**, *48*, 60–74.
4. Tang, Y.; Ouyang, M. Tailoring Properties and Functionalities of Metal Nanoparticles through Crystallinity Engineering. *Nat. Mater.* **2007**, *6*, 754–759.
5. Feldheim, D. L. The New Face of Catalysis. *Science* **2007**, *316*, 699–700.
6. Tian, N.; Zhou, Z. Y.; Sun, S. G.; Ding, Y.; Wang, Z. L. Synthesis of Tetrahexahedral Platinum Nanocrystals with High-Index Facets and High Electro-oxidation Activity. *Science* **2007**, *316*, 732–735.
7. Herdeveld, R. V.; Hartog, F. The Statstics of Surface Atoms and Surface Sites on Metal Crystals. *Surf. Sci.* **1969**, *15*, 189–362.
8. Ding, Y.; Gao, Y.; Wang, Z. L.; Tian, N.; Zhou, Z. Y.; Sun, S. G. Facets and Surface Relaxation of Tetrahexahedral Platinum Nanocrystals. *Appl. Phys. Lett.* **2007**, *91*, 121901.
9. Habas, S. E.; Lee, H.; Radmilovic, V.; Somorjai, G. A.; Yang, P. Shaping Binary Metal Nanocrystals through Epitaxial Seeded Growth. *Nat. Mater.* **2007**, *6*, 692–697.
10. Wang, C.; Daimon, H.; Lee, Y.; Kim, J.; Sun, S. Synthesis of Monodisperse Pt Nanocubes and Their Enhanced Catalysis for Oxygen Reduction. *J. Am. Chem. Soc.* **2007**, *129*, 6974–6975.
11. Wang, C.; Daimon, H.; Onodera, T.; Koda, T.; Sun, S. H. A General Approach to the Size- and Shape-Controlled Synthesis of Platinum Nanoparticles and Their Catalytic Reduction of Oxygen. *Angew. Chem., Int. Ed.* **2008**, *47*, 3588–3591.
12. Li, C. C.; Sato, R.; Kanehara, M.; Zeng, H. B.; Bando, Y.; Teranishi, T. Controllable Polyol Synthesis of Uniform Palladium Icosahedra: Effect of Twinned Structure on Deformation of Crystalline Lattices. *Angew. Chem., Int. Ed.* **2009**, *48*, 6883–6887.
13. Wang, J. X.; Inada, H.; Wu, L.; Zhu, Y.; Choi, Y.; Liu, P.; Zhou, W. P.; Adzic, R. R. Oxygen Reduction on Well-Defined Core–Shell Nanocatalysts: Particle Size, Facet, and Pt Shell Thickness Effects. *J. Am. Chem. Soc.* **2009**, *131*, 17298–17302.
14. Zhang, Q. B.; Xie, J. P.; Yang, J. H.; Lee, J. Y. Monodisperse Icosahedral Ag, Au, and Pd Nanoparticles: Size Control Strategy and Superlattice Formation. *ACS Nano* **2009**, *3*, 139–148.
15. Xia, Y.; Xiong, Y. J.; Lim, B.; Skrabalak, S. E. Shape-Controlled Synthesis of Metal Nanocrystals: Simple Chemistry Meets Complex Physics? *Angew. Chem., Int. Ed.* **2009**, *48*, 60–103.
16. Gasteiger, H. A.; Kocha, S. S.; Sompalli, B.; Wagner, F. T. Activity Benchmarks and Requirements for Pt, Pt-Alloy, and Non-Pt Oxygen Reduction Catalysts for PEMFCS. *Appl. Catal., B* **2005**, *56*, 9–35.
17. Lim, B.; Jiang, M. J.; Camargo, P. H. C.; Cho, E. C.; Tao, J.; Lu, X. M.; Zhu, Y. M.; Xia, Y. Pd–Pt Bimetallic Nanodendrites with High Activity for Oxygen Reduction. *Science* **2009**, *324*, 1302–1305.
18. Stamenkovic, V. R.; Mun, B. S.; Arenz, M.; Mayrhofer, K. J. J.; Lucas, C. A.; Wang, G. F.; Ross, P. N.; Markovic, N. M. Trends in Electrocatalysis on Extended and Nanoscale Pt–Bimetallic Alloy Surfaces. *Nat. Mater.* **2007**, *6*, 241–247.
19. Adzic, R. R.; Zhang, J.; Sasaki, K.; Vukmirovic, M. B.; Shao, M.; Wang, J. X.; Nilekar, A. U.; Mavrikakis, M.; Valerio, J. A.; Uribe, F. Platinum Monolayer Fuel Cell Electrocatalysts. *Top. Catal.* **2007**, *46*, 249–262.
20. Peng, Z. M.; Yang, H. Synthesis and Oxygen Reduction Electrocatalytic Property of Pt-on-Pd Bimetallic Heteronanostructures. *J. Am. Chem. Soc.* **2009**, *131*, 7542–7543.
21. Ding, Y.; Chen, M.; Erlebacher, J. Metallic Mesoporous Nanocomposites for Electrocatalysis. *J. Am. Chem. Soc.* **2004**, *126*, 6876–6877.
22. Liang, H.; Zhang, H.; Hu, J.; Guo, Y.; Wan, L.; Bai, C. Pt Hollow Nanospheres: Facile Synthesis and Enhanced Electrocatalysts. *Angew. Chem., Int. Ed.* **2004**, *43*, 1540–1543.
23. Yang, J.; Lee, J. Y.; Chen, L. X.; Too, H. P. A Phase-Transfer Identification of Core-Shell Structures in Ag–Pt Nanoparticles. *J. Phys. Chem. B* **2005**, *109*, 5468–5472.
24. Teng, X.; Liang, X.; Maksimuk, S.; Yang, H. Synthesis of Porous Platinum Nanoparticles. *Small* **2006**, *2*, 249–253.
25. Chen, G.; Xia, D.; Nie, Z.; Wang, Z.; Wang, L.; Zhang, L.; Zhang, J. Facile Synthesis of Co–Pt Hollow Sphere Electrocatalyst. *Chem. Mater.* **2007**, *19*, 1840–1844.
26. Teng, X.; Maksimuk, S.; Frommer, S.; Yang, H. Three-Dimensional PtRu Nanostructures. *Chem. Mater.* **2007**, *19*, 36–41.
27. Chen, H. M.; Liu, R. S.; Lo, M. Y.; Chang, S. C.; Tsai, L. D.; Peng, Y. M.; Lee, J. F. Hollow Platinum Spheres with Nanochannels: Synthesis and Enhanced Catalysis for Oxygen Reduction. *J. Phys. Chem. C* **2008**, *112*, 7522–7526.
28. Guo, S.; Dong, S.; Wang, E. A General Method for the Rapid Synthesis of Hollow Metallic or Bimetallic Nanoelectrocatalysts with Urchinlike Morphology. *Chem.—Eur. J.* **2008**, *14*, 4689–4695.
29. Xu, C.; Wang, L.; Wang, R.; Wang, K.; Zhang, Y.; Tian, F.; Ding, Y. Nanotubular Mesoporous Bimetallic Nanostructures with Enhanced Electrocatalytic Performance. *Adv. Mater.* **2009**, *21*, 2165–2169.
30. Yang, J.; Sargent, E. H.; Kelley, S. O.; Ying, J. Y. A General Phase-Transfer Protocol for Metal Ions and Its Application in Nanocrystal Synthesis. *Nat. Mater.* **2009**, *8*, 683–689.
31. Peng, Z.; Wu, J.; Yang, H. Synthesis and Oxygen Reduction Electrocatalytic Property of Platinum Hollow and Platinum-on-Silver Nanoparticles. *Chem. Mater.* **2010**, *22*, 1098–1106.

32. Stamenkovic, V. R.; Fowler, B.; Mun, B. S.; Wang, G. F.; Ross, P. N.; Lucas, C. A.; Markovic, N. M. Improved Oxygen Reduction Activity on $Pt_3Ni(111)$ *via* Increased Surface Site Availability. *Science* **2007**, *315*, 493–497.
33. Zhang, J.; Sasaki, K.; Sutter, E.; Adzic, R. R. Stabilization of Platinum Oxygen-Reduction Electrocatalysts Using Gold Clusters. *Science* **2007**, *315*, 220–222.
34. Hong, J. W.; Kang, S. W.; Choi, B.-S.; Kim, D.; Lee, S. B.; Han, S. W. Controlled Synthesis of Pd−Pt Alloy Hollow Nanostructures with Enhanced Catalytic Activities for Oxygen Reduction. *ACS Nano* **2012**, *6*, 2410–2419.
35. Strasser, P.; Koha, S.; Greeley, J. Voltammetric Surface Dealloying of Pt Bimetallic Nanoparticles: An Experimental and DFT Computational Analysis. *Phys. Chem. Chem. Phys.* **2008**, *10*, 3670–3683.
36. Chen, S.; Ferreira, P. J.; Sheng, W. C.; Yabuuchi, N.; Allard, L. F.; Shao-Horn, Y. Enhanced Activity for Oxygen Reduction Reaction on "Pt_3CO" Nanoparticles: Direct Evidence of Percolated and Sandwich-Segregation Structures. *J. Am. Chem. Soc.* **2008**, *130*, 13818–13819.
37. Koenigsmann, C.; Santulli, A. C.; Gong, K.; Vukmirovic, M. B.; Zhou, W.-P.; Sutter, E.; Wong, S. S.; Adzic, R. R. Enhanced Electrocatalytic Performance of Processed, Ultrathin, Supported Pd Pt Core Shell Nanowire Catalysts for the Oxygen Reduction Reaction. *J. Am. Chem. Soc.* **2011**, *133*, 9783–9795.
38. Liu, L.; Pippel, E. Low-Platinum-Content Quaternary PtCu-CoNi Nanotubes with Markedly Enhanced Oxygen Reduction Activity. *Angew. Chem., Int. Ed.* **2011**, *50*, 2729–2733.
39. Mazumder, V.; Chi, M.; More, K. L.; Sun, S. Core/Shell Pd/FePt Nanoparticles as an Active and Durable Catalyst for the Oxygen Reduction Reaction. *J. Am. Chem. Soc.* **2010**, *132*, 7848–7849.
40. Yang, H. Platinum-Based Electrocatalysts with Core−Shell Nanostructures. *Angew. Chem., Int. Ed.* **2011**, *50*, 2674–2676.
41. Reyes-Gasga, J.; Tehuacanero-Nunez, S.; Montejano-Carrizales, J. M.; Gao, X. X.; Jose-Yacaman, M. Analysis of the Contrast in Icosahedral Gold Nanoparticles. *Top. Catal.* **2007**, *46*, 23–30.
42. Ling, T.; Xie, L.; Zhu, J.; Yu, H. M.; Ye, H. Q.; Yu, R.; Cheng, Z.; Liu, L.; Yang, G. W.; Cheng, Z. D.; *et al.* Icosahedral Face-Centered Cubic Fe Nanoparticles: Facile Synthesis and Characterization with Aberration-Corrected TEM. *Nano Lett.* **2009**, *9*, 1572–1576.
43. Zhang, Q. B.; Lee, J. Y.; Yang, J.; Boothroyd, C.; Zhang, J. X. Size and Composition Tunable Ag−Au Alloy Nanoparticles by Replacement Reactions. *Nanotechnology* **2007**, *18*, 245605.
44. Radmilovic, V.; Gasteiger, H. A.; Ross, P. N. Structure and Chemical-Composition of a Supported Pt−Ru Electrocatalyst for Methanol Oxidation. *J. Catal.* **1995**, *154*, 98–106.
45. Yang, J.; Lee, J. Y.; Deivaraj, T. C.; Too, H. P. Improved Procedure for Preparing Smaller and Nearly Monodispersed Thiol-Stabilized Platinum Nanoparticles. *Langmuir* **2003**, *19*, 10361–10365.
46. Markovic, N.; Gasteiger, H.; Ross, P. N. Kinetics of Oxygen Reduction on Pt(hkl) Electrodes: Implications for the Crystallite Size Effect with Supported Pt Electrocatalysts. *J. Electrochem. Soc.* **1997**, *144*, 1591–1597.
47. Li, H. Q.; Xin, Q.; Li, W. Z.; Zhou, Z. H.; Jiang, L. H.; Yang, S. H.; Sun, G. Q. An Improved Palladium-Based DMFCS Cathode Catalyst. *Chem. Commun.* **2004**, *23*, 2776–2777.
48. Hayre, R. O.; Cha, S. W.; Colella, W.; Prinz, F. B. *Fuel Cell Fundamentals*; John Wiley & Sons, Inc.: New York, 2006.
49. Bligaard, T.; Norskov, J. K. Ligand Effects in Heterogeneous Catalysis and Electrochemistry. *Electrochim. Acta* **2007**, *52*, 5512–5516.
50. Marković, N. M.; Ross, P. N. Surface Science Studies of Model Fuel Cell Electrocatalysts. *Surf. Sci. Rep.* **2002**, *45*, 117–229.
51. Zhang, J.; Vukmirovic, M. B.; Sasaki, K.; Nilekar, A. U.; Mavrikakis, M.; Adzic, R. R. Mixed-Metal Pt Monolayer Electrocatalysts for Enhanced Oxygen Reduction Kinetics. *J. Am. Chem. Soc.* **2005**, *127*, 12480–12481.
52. Zhang, J.; Vukmirovic, M. B.; Xu, Y.; Mavrikakis, M.; Adzic, R. R. Controlling the Catalytic Activity of Platinum-Monolayer Electrocatalysts for Oxygen Reduction with Different Substrates. *Angew. Chem., Int. Ed.* **2005**, *44*, 2132–2135.
53. Xu, Y.; Ruba, A. V.; Mavrikakis, M. Adsorption and Dissociation of O_2 on Pt−Co and Pt−Fe Alloys. *J. Am. Chem. Soc.* **2004**, *126*, 4717–4725.
54. Stamenkovic, V.; Schmidt, T. J.; Ross, P. N.; Markovic, N. M. Surface Composition Effects in Electrocatalysis: Kinetics of Oxygen Reduction on Well-Defined Pt_3Ni and Pt_3Co Alloy Surfaces. *J. Phys. Chem. B* **2002**, *106*, 11970–11979.
55. Markovic, N. M.; Ross, P. N. *Interfacial Electrochemistry: Theory, Experiment, and Applications*; Andrzej, W., Ed.; Marcel Dekker, Inc.: New York, 1999; p 827.
56. Somorjai, G. A. *Introduction to Surface Chemistry and Catalysis*; Wiley: New York, 1994.